Non-Interceptive Beam Current and Position Monitors for a Cyclotron Based Proton Therapy Facility

Srinivasan, Sudharsan

DOI:
10.33612/diss.149817352

Chapter 2: Design and Simulation of a Dielectric-filled Reentrant Cavity Resonator as Proton Beam Current Monitor

This Chapter is summarized in the following paper:

Srinivasan, S.; Duperrex, P.-A. Dielectric-filled Reentrant Cavity Resonator as a Low-Intensity Proton Beam Diagnostic. *Instruments* **2018**, *2*, 24
Doi: https://doi.org/10.3390/instruments2040024.

2.1 Introduction

In the previous Chapter, we discussed that cavity resonators find their use in most of the accelerator facilities thanks to their ability to measure low beam current and to deliver a high signal sensitivity, compared to other non-invasive diagnostic devices. When excited by a passing charged particle bunch, specific field configurations resonate within the cavity at specific frequencies. For the beam current measurement, we want to excite the cavity at a specific resonant mode known as the monopole mode (TM_{010}). We have designed a cavity that the resonance frequency of this mode coincides with the frequency of the 2^{nd} harmonic of the beam pulse repetition rate of 72.85 MHz, i.e., at 145.7 MHz. Since the resonator consists of a closed metal structure, the induced electromagnetic fields oscillate within that boundary [1]. We can realize such a cavity either in the form of a pillbox cavity or a reentrant coaxial cavity, as shown in Figure 2.1. However, before we decide whether to use a pillbox cavity or a reentrant coaxial cavity, it is important to understand the fundamentals of this monopole mode.

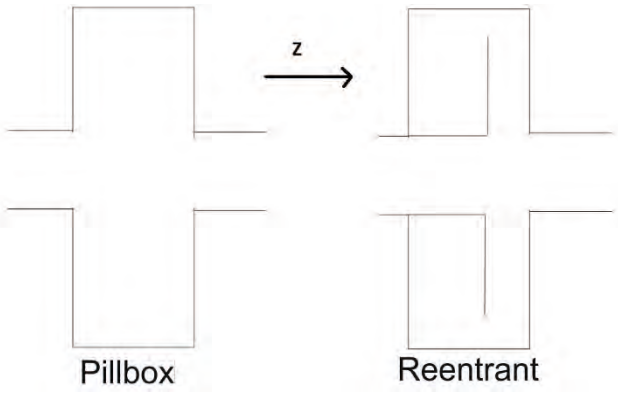

Figure 2.1: Outline of a pillbox and a reentrant coaxial cavity.

2.1.1 Maxwell equations in a simple pillbox RF Cavity

Since we wish to design the cavity resonator in a cylindrical form, the fields of the excited mode can be solved in cylindrical coordinates (r,φ,z) with Maxwell's equations in their differential form as given in [1], [2]. Resonating cavities classified by electromagnetic modes can be represented as Transverse Magnetic (TM_{mnp}) and Transverse Electric (TE_{mnp}) mode cavities [1]. In cylindrical coordinates, these indices m, n, p represent as defined by:

- (m=0) Zero full period sinusoidal variation of the field components along the azimuthal direction.
- (n=1) One zero crossing of the longitudinal field components in the radial direction.
- (p=0) Zero half-period sinusoidal variation of the field components in the longitudinal direction.

The simplest solution for the standard wave equations given in [3] for a circular geometry (cylindrical cavity) of radius R and length L that has an axial electric field is the TM_{010} mode. A cylindrical cavity can be regarded as a section of a cylindrical waveguide [4]. The Eigen frequency of the waveguide is independent of the cavity length.
Since the TM_{010} mode has no axial dependence, for a simple cavity closed at Z = 0 and Z = L and with a radius r = a with perfectly conducting walls, the axial electric and azimuthal magnetic fields are given as in [4]

$$E_z = \frac{1}{j\omega\varepsilon_o}\frac{\chi_{01}}{a}\sqrt{\frac{1}{\pi}}\frac{J_o\left(\frac{\chi_{01}}{a}r\right)}{aJ_1\left(\frac{\chi_{01}}{a}\right)}$$
$$B_\varphi = \mu_o\sqrt{\frac{1}{\pi}}\frac{J_o\left(\frac{\chi_{01}}{a}r\right)}{aJ_1\left(\frac{\chi_{01}}{a}\right)} \quad (2.1)$$

Here χ_{01} is the first zero-crossing of the Bessel function J_o. The resonance frequency of the mode TM_{010} is then given by

$$f_{010} = \frac{c}{2\pi}\left(\frac{\chi_{01}}{a}\right) \quad (2.2)$$

where, $\chi_{01} = 2.405$.

The Bessel function of the order m = 0 has a weak dependence on the radius r close to the cavity center since the derivative of the Bessel function is zero for r = 0. Hence, the monopole mode TM_{010} amplitude is proportional to the beam charge independent of its position close to the cavity center [5]. The field configuration of the TM_{010} mode is as shown in Figure 2.2.

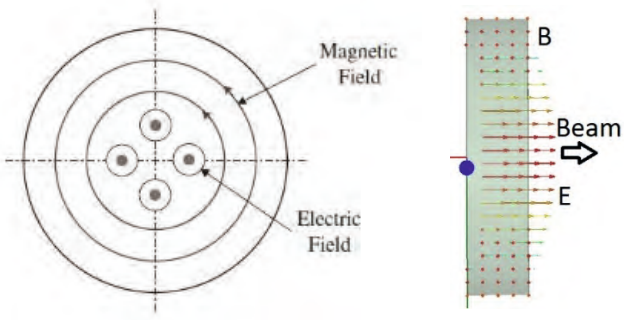

Figure 2.2. Fields of the Monopole mode in a simple pillbox cavity [6].

For a design resonance frequency of 145.7 MHz, we can calculate the radius of the pillbox cavity from Eq. (2) as $r = a = 0.78$ m.

Since we are limited to a confined space in the beamlines of COMET, a simple pillbox cavity is not suitable due to its large transversal size. Hence, we need to build a more compact system that still delivers a bunch charge information based on the TM_{010} mode. We can achieve this by constructing a cavity as a lumped element circuit such as an LC resonator [7]. This is equivalent to a coaxial cavity with a short-circuit at one end and a capacitively-loaded gap at the other end [8].

The walls of the coaxial structure then act as a distributed inductance. We summarize in the next section its working principle and the transmission line analogy, which helps to evaluate first-order dimensions of a reentrant coaxial cavity.

2.1.2 Approximation of the coaxial cavity from an LC model

The reentrant coaxial cavity resonator is modeled by evolution from the lumped element model. The lumped element model with the ideal coupling loop and the current source is as shown in Figure 2.3. The translation of the lumped element model into a geometrical structure results in a physical picture of a reentrant coaxial cavity, as shown in Figure 2.4. In the reentrant coaxial cavity, there is a Transverse Electromagnetic (TEM) field configuration in the separate transmission lines (coaxial line and the radial line, see Figure 2.9). However, due to the cavity's geometry, the field distribution in the coaxial cavity is a quasi-TEM, similar to when a coaxial line will be bent or in the case of inhomogeneous dielectric in the cavity as described in [9].
As expressed in [10], the TEM mode field configuration in the radial line section (reentrant capacitive part) of the coaxial cavity can be approximated as the TM_{010} mode in a circular cylindrical cavity such as a pillbox since the field solutions are the same. Moreover, at resonance, the capacitor plates (C_{gap}) retains the majority of the induced electric field, and the cavity walls acting as the coaxial inductor (L_{coax}) retain most of the induced magnetic field as discussed by Feynman [7]. Moreover, we have observed that the signal level for a given beam current from the TM_{010} mode analysis matches the simulation estimate (shown later in this Chapter) and the measurement (Chapter 3). Thus, we approximate the fields in the cavity by the TM_{010} mode.

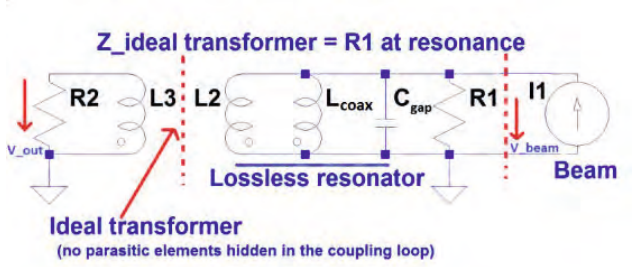

Figure 2.3: Lumped element circuit of an LC resonator with an ideal coupling loop represented as an ideal transformer. I1is current source with infinite impedance, R1 represents resonator losses, R2 represents output impedance, the mutual inductance between the two inductances L2 and L3 represent ideal transformer coupling.

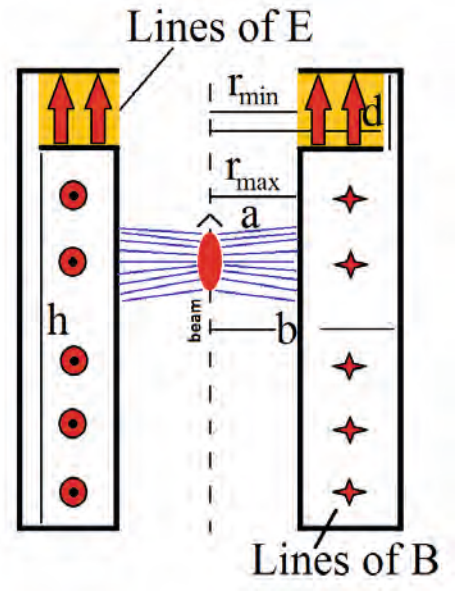

Figure 2.4: Reentrant Coaxial Cavity transition from an LC resonator. Relevant field configurations are shown here as an approximation of the TM_{010} mode. The complete field distributions of the TEM modes can be seen in Figure 2.9.

The impedance of the equivalent circuit (of the coaxial cavity) is given by

$$Z(\omega)=\frac{1}{\frac{1}{R1}+\frac{1}{j\omega L_{coax}}+j\omega C_{gap}} \tag{2.3}$$

For a loaded gap capacitance, C_{gap} (because of the central hole) is given by

$$C_{gap}=\frac{\varepsilon_r \varepsilon_o \pi\left(r_{max}^2 - r_{min}^2\right)}{d} \tag{2.4}$$

with r_{max} and r_{min} being the outer and inner radius of the capacitor plates and d is the gap between the two plates. ε_r is the relative permittivity of the material filling the gap, and ε_o is the vacuum permittivity.

The angular resonance frequency is then given by

$$\omega_o = \frac{1}{\sqrt{L_{coax} C_{gap}}} \tag{2.5}$$

An improved estimate of the resonance frequency and the dimensions of a reentrant coaxial cavity are determined from the properties of a coaxial transmission line as given below, which is a summary from [11]. Here the inner radius of the outer conductor is b, the outer radius of the inner conductor is a, length of the coaxial line is h, ε_r the relative permittivity of the dielectric in the coaxial section. The magnetic circuit formed by the cylindrical sleeves of the coaxial transmission line contributes L_{coax}, the equivalent inductance. The expressions for the inductance, capacitance, and characteristic impedance (Z_o) of a coaxial transmission line (see Figure 2.4) can be found in Feynman [7].

The general expression to evaluate the input impedance of a lossless coaxial line can be found in [12].

Since one end of the coaxial line is shorted, the load impedance is $Z_L = 0$, and the above equation takes the form

$$Z_i = j Z_o \tan\left(\frac{2\pi h}{\lambda_0}\right) \tag{2.6}$$

From the above equation, the impedance is an inductive reactance ($\tan(\frac{2\pi h}{\lambda_o})$ is positive) for length h smaller than $\lambda_o/4$. To obtain a reentrant coaxial cavity resonator, the input impedance of the coaxial line is compensated by the capacitive reactance of the gap C_{gap}, which gives the condition for resonance and is given by

$$\frac{2\pi h}{\lambda_0} = \arctan\left(\frac{\lambda_0}{2\pi c C_{gap} Z_o}\right) \tag{2.7}$$

where λ_o is the free-space wavelength and c is the propagation velocity.

The above equation for the transmission line length normalized to the desired free-space wavelength, h/λ_o, versus the free-space wavelength normalized to the loaded transmission line characteristics, $\lambda_o/2\pi c C_{gap} Z_o$, is plotted in Figure 2.5. From the above transmission line analogy, we find that for values of $\lambda_o/2\pi c C_{gap} Z_o$ ranging between (0.5-1.0), the normalized transmission line length h/λ_o varies in the range (0.10-0.15). Hence, any capacitive loading of an

LC cavity for a given size results in a reduction of the resonance frequency and thus a for a given resonance frequency [13] a reduction in size as compared to the unloaded case.

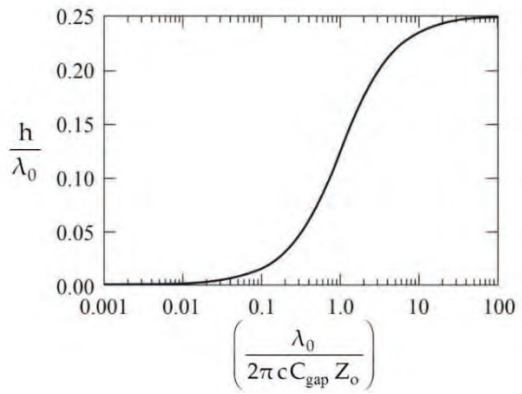

Figure 2.5: Universal tuning curve to determine the reentrant cavity resonator length normalized to the free-space wavelength of the microwave frequency in the resonator [11].

2.1.3 Cavity Parameters: Q (Quality Factor) and coupling coefficient

The beam current measurement is performed by coupling power out of the cavity resonator. The location, size, orientation, and the type of measurement probe (electric coupling, magnetic coupling, direct coupling or window coupling) as described in [14], determines the matching condition, which in turn affects the performance of the cavity. This characterization is based on the rate of energy loss of a resonator and is given by the Q (Quality) factor.

For an air-filled cavity made of a non-perfect conductor like aluminum or copper, the dominating losses at resonance are the ohmic losses, and in the presence of a lossy-dielectric in the cavity, the dominating losses are from the dielectric. Hence, the cavity exhibits a driven, damped harmonic oscillation.

Thus, a cavity is characterized for a given excited mode by its resonance frequency and its Q-factor[4]. It is defined as the ratio between the stored energy in the cavity resonator at any time and the energy dissipated per oscillation period [15, 16], which can be expressed as [17]:

$$Q_L = \left[\frac{\omega_o \, W_{max}}{P_{d=total} = P_{cond} + P_{diel} + P_{rad} + P_{ex}} \right]_{\omega=\omega_{res}} \tag{2.8}$$

where, W_{max} is the maximum energy stored in the resonator and P_d is the average dissipated power.

Thus, a term called loaded Q factor as Q_L (measurable Q) can be defined which takes into account the power lost in the conducting walls (P_{cond}), in lossy dielectrics (P_{diel}), in radiation (P_{rad}), and in external circuits (P_{ex}). Q factor measurements in the frequency domain are performed as the transmission type measurement [18], which provide the Q_L from the 3 dB bandwidth of the resonance frequency as

$$Q_L = \frac{\omega_0}{\Delta\omega_{3dB}} \tag{2.9}$$

The above Eq (2.8) can be then be written of the form

$$\frac{1}{Q_L} = \frac{1}{Q_0} + \frac{1}{Q_{ext}} \tag{2.10}$$

The unloaded Q factor, Q_o, depends purely on the geometry and materials for the construction of the resonator such that, with a shunt impedance R1 (see next section):

$$\frac{1}{Q_o} = \frac{P_{cond} + P_{diel}}{\omega_o W_{max}} = \frac{1}{\omega_o C_{gap} R1} \tag{2.11}$$

and Q_{ext} is the external Quality factor under the assumption the radiation loss is zero:

$$\frac{1}{Q_{ext}} = \frac{P_{ex}}{\omega_o W_{max}} \tag{2.12}$$

The coupling coefficient κ is defined as the ratio of coupling strength between the cavity and the external circuit and is given by

$$\kappa = \frac{Q_o}{Q_{ext}} \tag{2.13}$$

2.1.4 Beam cavity interaction

In this subsection, we provide an analytical formulation to estimate the output signal from a cavity resonator for a given bunch charge. When a bunched beam traverses an "empty" cavity, it transmits energy to the cavity through the electromagnetic field associated with the moving charge [19]. This energy loss of a charged particle by passing through the cavity and the stored energy gain of the cavity, are related to the properties of the cavity Eigenmodes. This allows calculating the amplitude of any given resonance mode of a cavity by the beam passing through it.

The voltage of a resonance mode excited in a cavity by a passing beam can be derived from [19]

$$V_{exc} = \omega_o \left(\frac{R1}{Q_o} \right) q \tag{2.14}$$

where q is the beam charge, and R1 represents the resonator losses, as shown in Figure 2.3. R1 is in circuit theory known as the shunt impedance and is given by

$$R1 \equiv \frac{\left| \int Eds \right|^2}{2P_{total}} \tag{2.15}$$

where E is the induced electric field of the resonance mode, ∫ds is the path length along the cavity gap, P_{total} is the total dissipation power of the cavity for the resonance mode. Thus, $R1/Q_o$ is the normalized shunt impedance, which characterizes the energy exchange between the beam and the cavity, is given by

$$\frac{R1}{Q_o} = \frac{\left| V_{exc} \right|^2}{2\ \omega_o W_{max}} \tag{2.16}$$

The above Eq (2.14) does not take into consideration the bunch length along the beam direction. When the bunch length (σ_z) is non-negligible compared to the wavelength of the excited mode, the effective signal amplitude is reduced. This is because particles in the bunch pass the cavity at different times, which induces a phase shift with respect to the excited mode during the passage. The total excited voltage of a resonance mode at a cavity for a gaussian shaped bunch is given by

$$V_{totalexc} = V_{exc} \exp(-\omega_o^2 \sigma_z^2 / 2\beta^2 c^2) \tag{2.17}$$

The maximum stored energy in a cavity can then be written as

$$W_{max} = \frac{V_{totalexc}^2}{2\ \omega_o \left(\frac{R1}{Q_o} \right)} = \frac{\omega_o}{2} \frac{R1}{Q_o} q^2 \exp(-\omega_o^2 \sigma_z^2 / \beta^2 c^2) \tag{2.18}$$

From Eq (2.10) P_{ex}, the power coupled out to the measurement device is then given by

$$P_{ex} = \frac{\omega_o W_{max}}{Q_{ex}} \tag{2.19}$$

Detecting this power over an impedance Z gives the peak output voltage as

$$V_{out} = \sqrt{2ZP_{ex}} \equiv \omega_o q \sqrt{\frac{Z}{Q_{ex}} \frac{R1}{Q_o}} \exp(-\omega_o^2 \sigma_z^2 / 2\beta^2 c^2) \tag{2.20}$$

The analytical estimate from subsections 2.1.2, 2.1.3, and 2.1.4 gives approximate dimensions of the cavity resonator, quality factors, and expected output voltage for a given resonance frequency. A full simulation is needed to obtain accurate results.

2.2 Second harmonic matching

For the PROSCAN situation, with a bunch repetition rate of 72.85 MHz, we chose one of the harmonics as the resonance frequency to prevent direct background contributions from the cyclotron accelerating cavities. The second harmonic, i.e., 145.7 MHz, is chosen since it contains more energy than the higher harmonics. Moreover, for smaller harmonics, their relative contribution is less affected by changes in the bunch shape compared to higher harmonics.

Before we design the reentrant coaxial resonator at the design frequency of 145.7 MHz, we estimate the available signal level of the 2nd harmonic at the cavity. We assume a rectangular pulse of length 2 ns as the proton bunch length (expected at the degrader exit). The Fourier spectrum of this bunch will provide the value of the harmonic component contributions represented as the amplitude of the Sinc function. The various harmonic components of the signal are directly proportional to the beam current [20]:

$$X_n = \frac{A\Delta}{T}\frac{\sin(n\Delta/T)}{n\Delta/T} \tag{2.21}$$

where X_n is the harmonic component contribution, A the amplitude of the bunch, Δ the bunch length, T the bunch repetition period, and n the harmonic. $A\Delta$ is the pulse area, hence is proportional to the number of protons (bunch charge) and $A\Delta/T$ is proportional to the beam intensity. The amplitude of the various harmonics, calculated according to Eq (2.21), is shown in Figure 2.6 for two scenarios, where the bunch length is 2 ns and 4 ns, respectively, for a bunch repetition period T of 13.72 ns (corresponding to 72.85 MHz). This highlights how the increase in the bunch length along the beamline when the beam has energy spread can reduce the harmonic components in the bunch structure. With decreasing energy, this effect will become larger due to a larger beam energy spread created in the degrader. Thus, there will be an energy spread dependent decrease in the beam-induced signal.

The location of the cavity resonator in the beamline will therefore play a role in determining the amount of beam signal available for excitation of the cavity at the design resonance frequency of 145.7 MHz. A detailed discussion of the second harmonic dependence on bunch length elongation is given in the next Chapter on measurements with a beam.

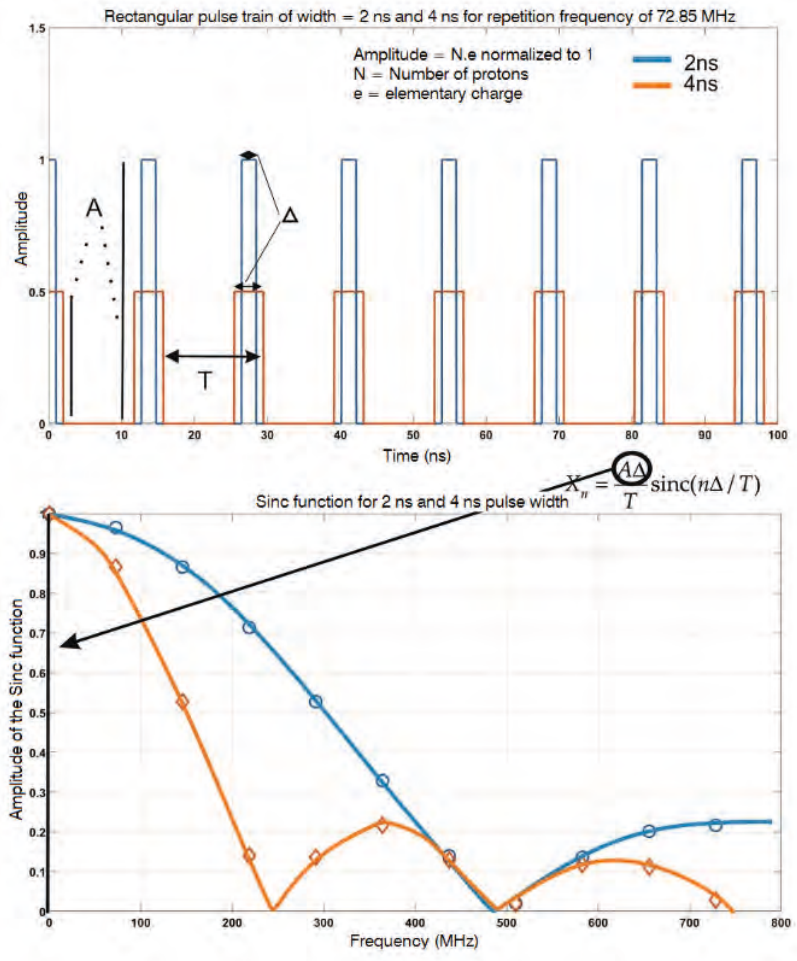

Figure 2.6: Plots representing 2 ns and 4 ns bunch width at the same beam intensity with a repetition rate of 72.85 MHz and its corresponding Fourier series represented as Sinc function. $A\Delta$ is maintained constant.

2.3 Simulation objective

Since in PROSCAN, we are dealing with beam currents in the range 0.1-10 nA, the design consideration for the cavity resonator is to deliver maximum beam induced signal to the measurement electronics. The cavity parameters are generally measured with the help of a network analyzer via a two-port measurement (transmission coefficient for a multiple port device). Hence, the goal is to simulate the network analysis of the cavity and optimize the design for maximum pickup signal from the beam at the required frequency.

The transmission coefficient between beam and measurement signal expressed as Scattering parameter S_{ji} (between i = input port, j = output port) in terms of the loaded and unloaded quality factor is given by

$$\left|S_{ji\,,ij}\right| = 1 - \frac{Q_L}{Q_o} \tag{2.22}$$

The S_{ji} plot (see Figure 2.7) is a graphical representation for lower vs higher loaded quality factor. By coupling-out more signal power from a measurement port, the loaded quality factor is expected to reduce. In such a scenario, a resonance frequency offset of a few 100 kHz from the design demands would not have a strong influence on the transmission coefficient. For a real cavity, a resonance frequency offset of a few 100 kHz due to machining tolerances and assembly errors can generally be accepted. Moreover, in unforeseen circumstances where the temperature stability could not be maintained, the cavity dimensions or the properties of the filling of the cavity (such as a dielectric) could be affected due to thermal loading, which can result in shifting of the resonance frequency. A system with a lower loaded Q provides a safety window in such a situation.

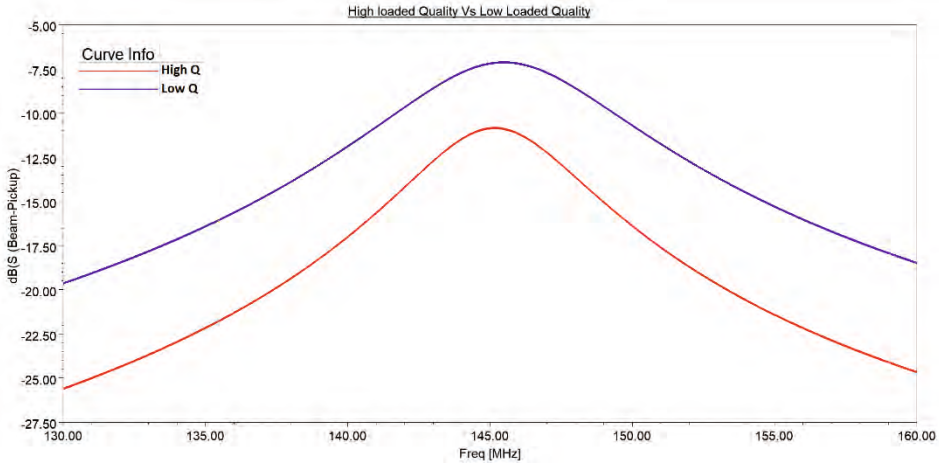

Figure 2.7: Higher vs lower loaded Q factors from the $S_{beam\text{-}pickup}$ transmission plots.

Considering the above factors, the cavity resonator should be designed to have maximum pickup coupling for a beam excitation, to have a higher output signal into the measurement electronics.

2.4 ANSYS HFSS

ANSYS HFSS is a High-Frequency Structure Simulator [21], which we use to design the reentrant coaxial resonator. The solution to the model is derived from

the differential form of Maxwell's equations. We chose ANSYS HFSS as it is a high-performance full-wave electromagnetic field simulator. HFSS integrates simulation, visualization, and solid modeling, which provides accurate results, and is therefore used for design and network analysis of the reentrant coaxial cavity resonator prototype.
The workflow of the HFSS involves the following:

- Parametric model generation: geometry, boundaries, excitations
- Analysis setup: solution setup and frequency sweeps
- Results: reports and field plots
- Solve loop: automation of the solution process

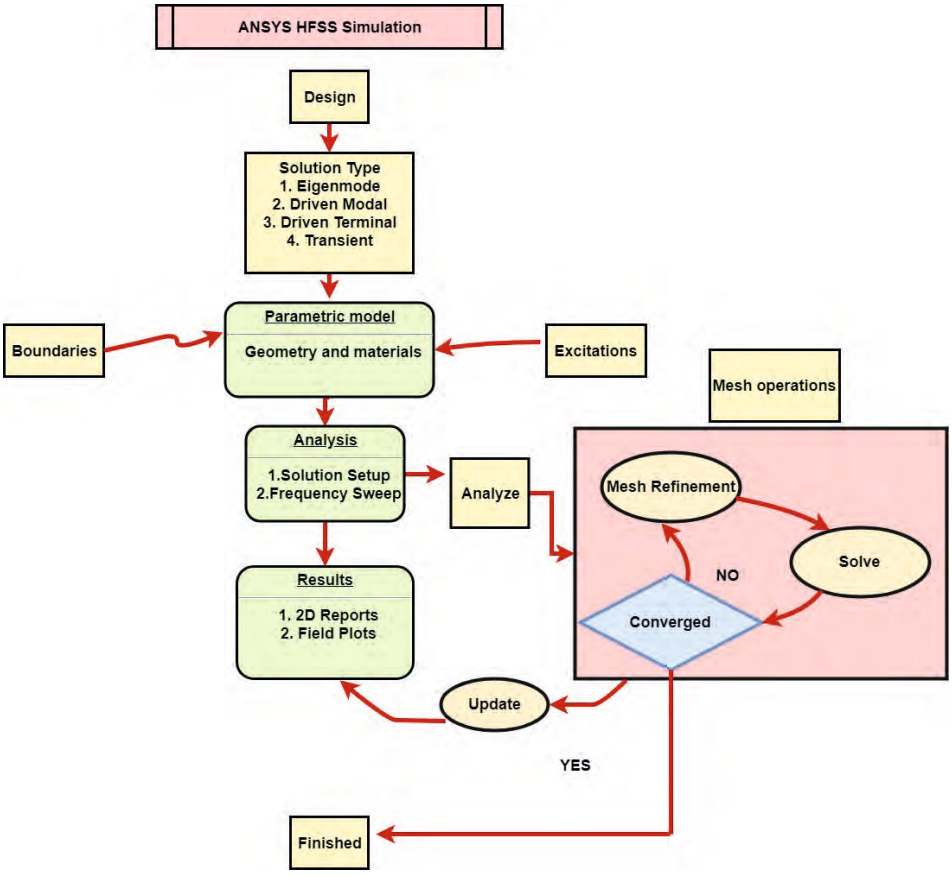

Figure 2.8: HFSS workflow for the simulation process to solve a model.

From the above Figure 2.8, two solution types that are used for the design and characterization of the cavity resonator are:

- Eigenmode solution type to identify Eigenmodes or resonance frequencies, unloaded quality factor, and EM-fields associated with the model at those frequencies. The criteria for convergence of the solution is the condition that the calculated resonance frequency differs less than 0.01% for the desired resonance frequency.
- Driven modal solution type to provide Scattering (S) - parameters for intra-pickup coupling, beam-pickup coupling, and the loaded quality factor. The criteria for convergence of solution between two successive iterations is given by $\Delta|S_{ji}| \leq 0.02$ dB.

2.4.1 Design overview

As mentioned in previous subsection 2.1.2, we design a coaxial resonator taking into consideration certain dimensional limitations, choice of material, and choice of dielectric filling. The objective for the choice of material and dielectric filling is to keep the manufacturing process simple and its costs low, as it is a proof of principle prototype.

Limitation of certain dimensions

The PROSCAN beamline has a beam pipe of radius 45 mm. To install the reentrant cavity resonator in the beamline, we need the waveguide sections (i.e., cavity extensions on entry and exit ports) to match with the beam pipe dimensions. To provide easy installation of the prototype, the inner coaxial cylinder is chosen with a radius of 50mm. Since the inner coaxial cylinder will also support the capacitor plate at one end, we choose the inner radius of the dielectric ring also as 50 mm.

Choice of metal

The material from which the resonator is built has to contain the field (shielding) and therefore, should have the highest possible electrical conductivity. The standard choice of material to build such resonators generally should possess high conductivity, good mechanical resilience, and high mechanical rigidity. At higher frequencies (tens of MHz and beyond), the RF shielding effectiveness is a function of seam and penetration integrity, which is mainly affected by assembly and machining techniques [21]. Due to this fact, the two most commonly used materials are copper and aluminum. Aluminum is chosen for the construction of the resonator due to its better strength-to-weight ratio and lower costs.

Choice of the dielectric filling (Reentrant gap)

The loaded gap capacitance that terminates the coaxial line determines the required value of the inductance and can be used to determine the dimensions of the coaxial line according to Eq (2.7). Vice-versa, for a given length of the coaxial part (and its characteristic impedance Z_o), the gap capacitance can be chosen to tune the resonance frequency given by Eq (2.4) and Eq (2.5).

For a vacuum-filled coaxial resonator to be installed within a given length in the beamline, the reentrant gap (i.e., capacitive loading) can be designed either as a large capacitance (transverse space costs) or as a small capacitance (longitudinal costs). Similarly, the coaxial impedance could be used to optimize the LC resonator design at similar expenses as above.

However, by choosing to fill the reentrant gap with a dielectric, whose dielectric constant is higher than that of vacuum, we can establish relaxed machining and assembly tolerance of the capacitive gap in the resonator. Moreover, we can tune resonance frequency offset corrections as per Eq (2.4) by adjusting the dimensions of the dielectric. For instance, with a fixed reentrant gap (i.e., dielectric thickness), the cross-sectional area of the dielectric can be altered to match the resonance frequency and vice-versa.

For the choice of dielectric, we chose macor ceramic over alumina ceramic (its closest competitor), as macor is readily available, cheaper, and can be easily machined compared to alumina ceramic due to its low hardness. We summarize the relevant material properties for the construction of the resonator in Table 2.1.

Table 2.1: Important material properties of aluminum (taken from HFSS material library) and macor as provided by the supplier [22].

Properties	**Aluminum**	**Macor**
Bulk Conductivity, S/m	3.8E+07	-
Relative Permittivity, ε_r	1	6.0 at 1 kHz
Relative Permeability, μ_r	1.000021	1
Dielectric Strength, kV/mm	-	45
Loss tangent	-	0.005 at 1kHz

We can evaluate multiple combinations of dimensions to match the resonance frequency of 145.7 MHz. By taking into consideration the universal tuning curve Figure 2.5, an overall compact system can be achieved by predefining the gap capacitance in the range of a few pF. Higher values of gap capacitance will not provide a compact system in transverse space.

With these above-mentioned geometrical limitations, we will evaluate the other dimensions of the resonator with the help of Eigenmode and Driven Modal solutions.

2.4.2 Eigenmode Solution Setup

A gap capacitance of 50 pF is assumed as the reference to evaluate the primary dimensions. Using Figure 2.5 and the standard coaxial inductance equation, we evaluate the effective inductance of the coaxial line in the range of 20 nH. With these values for the gap capacitance and the coaxial inductance, an isolated resonator (i.e., no pickup ports), is designed to match the resonance frequency and to evaluate the unloaded Q. The solution setup used for solving the model is summarized in Table 2.2. The description of how the Eigenmode solver finds the resonance frequencies and their field configurations can be found in [24]. Here, the Eigenmode solutions provide the unloaded Q taking into consideration all the power loss terms mentioned in subsection 2.1.3 except the P_{ex} term.

Table 2.2: Summary of the solution setup model. Included are some of the fundamental derived design parameters. B – Beam pipe diameter, d – inner diameter of the inner coaxial cylinder, C – outer diameter of the macor ring, t – dielectric thickness, W – outer diameter of the capacitor plate, D – inner diameter of the outer coaxial cylinder, M – air dielectric thickness in the coaxial line section.

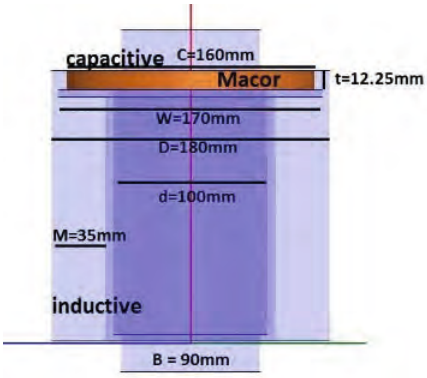

Materials	**Vacuum, Macor**	
Boundaries	Aluminum finite conductivity on faces	
Excitation	None for Eigenmode	
Mesh Operations	Curvilinear, Skin-depth on Tau mesher	
Analysis	Minimum Frequency	100 MHz
	No. of Modes	1
	No. of passes	20
	Convergence, Δf	0.01%
	Initial Mesh	λ refinement
	Refinement per pass	20%
	Order of Basis functions (solutions)	2nd order
Results	E, H plots, Resonance Frequencies, Q_0	

The maximum stored energy, $W_{max} \approx 10^{-16}$ J, is calculated by integrating the electric field and its conjugate within the cavity volume. The losses associated with the cavity metal ($P_{cond} \approx 10^{-11}$ W) and the dielectric ($P_{diel} \approx 10^{-10}$ W) are calculated by integrating the surface loss density over the cavity metal surface and the volume loss density over the dielectric volume from the HFSS solutions. The number of modes the solver has to determine is limited to one as we are interested in the fundamental mode only. For accurate results from the model, the convergence criteria for the model is chosen as the Δ frequency $\leq 0.01\%$.

Results

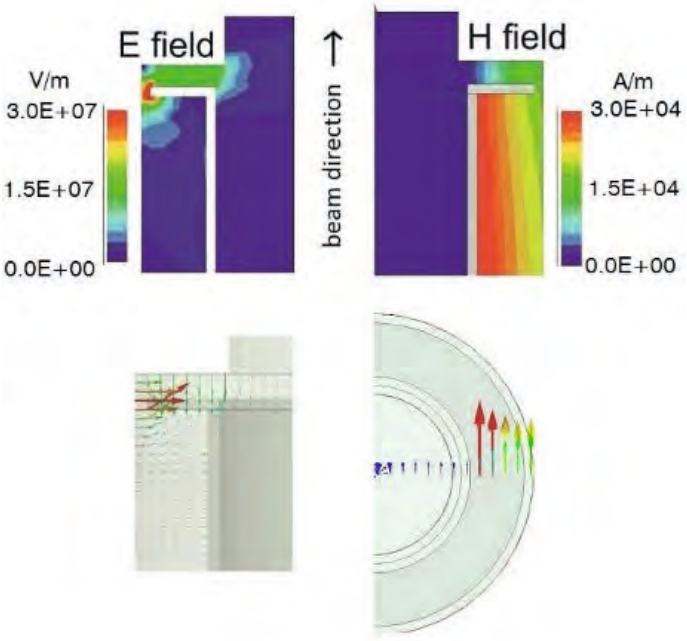

Figure 2.9: E and H field (both magnitude and vector) configurations of the reentrant coaxial cavity at resonance. In the separate transmission lines of the cavity (coaxial and radial), the field configuration is of a TEM wave.

The Eigenmode solver gives the fundamental resonance at 145.7 MHz with an unloaded Q as $Q_0 \approx 267$ for the above model corresponding to Eq (2.11). We clearly observe the influence of macor in the reentrant gap. By solving the same model without macor, the resonance frequency of 225.0 MHz and an unloaded Q, $Q_o = 5085$, is achieved for the model. The reduction in the Q_o by the insertion of the macor in the reentrant gap shows it is a lossy dielectric (dissipation of energy in an alternating electromagnetic field), and as a result, more power is lost compared to lossless. Thus, it is important to minimize internal losses of the cavity for the future design considerations.
However, prior to fine-tuning the model in the Driven modal setup, it is necessary to confirm that the excited mode of resonance is the desired mode. This we can confirm by plotting the E and H magnitude and vector plots in Figure 2.9.
We fine-tune the resonator using the Driven modal solver, which takes into account the presence of a beam analogon and the influence of multiple inductive pickups.

2.4.3 Driven modal Solution Setup

In the previous subsection, we evaluated the primary dimensions of our prototype but as an isolated cavity. The solutions of the Driven modal provides us with transmission or reflection coefficients S_{ji} (scattering parameters) and quantifies how RF energy propagates in a multi-port network. These values will provide us with information on the amount of signal that could be coupled out of the cavity. This provides information on the external quality factor of the cavity as per Eq (2.10). To study the resonator under the influence of beam, we cannot define an actual beam, so we use a beam analogon, i.e., a straight wire of a perfect electric conductor with a small diameter to minimize capacitive coupling between the wire and the inner coaxial cylinder. By placing the stretched wire at the center of the cavity, we put the beam equivalent excitation in the center of the beamline. Generally, signals are coupled out either with an antenna or a loop. An antenna is used to couple to the electric field, while a loop couples to the magnetic field. If we choose an antenna, we have to place it such that it protrudes in the reentrant zone where the maximum electric field exists. We can then calculate the voltage coupled out of the cavity as

$$V=\int \vec{E}.\vec{dl} \tag{2.23}$$

If we choose a loop, we have to place it in the inductive zone. From the field plots in the previous section, we clearly see that the inductive zone provides more freedom to locate the loops along the length of the coaxial line section. Moreover, we can design a loop of any shape. The voltage coupled out is given by

$$V=\int_A \frac{d\vec{B}}{dt}\bullet d\vec{a} \tag{2.24}$$

where A is the area of the loop, and the signal level is expected in the range of nV for beam currents in the range of nA. Hence, an inductive loop is chosen to couple out information. We wish to have four loops, two large and two small loops, since in our prototype, we want more flexibility in the operation of the resonator in cases where if the measurement pickup does not function properly due to connection issues. A large loop is designated as a measurement port and the other large loop could be used as a resonance trombone, which is a constant impedance adjustable coaxial line, to tune the resonance frequency offsets. In practice, we can achieve this by attaching a simple coaxial RF cable and cut it at the required length. We will use the smaller loops for online verification of the functioning of the cavity.

The next question in the design is to find the location of these pickups in the resonator, especially the larger pickups, to couple out maximum signal power. Since inserting pickups adds insertion loss, we expect it to somewhat modify the resonance frequency at which the maximum power is transferred to the measurement system. The location and the size of the loops play a role in determining maximum power transfer from beam-induced signals.
Network analysis is performed to achieve maximum power transfer from the beam with a parametric investigation of the resonator dimensions such as pickup position, dielectric width, and thickness

Parametric Model

The parametric geometry from the Eigenmode solver is imported into the Driven modal setup. The location of the pickups is defined in the Driven modal also parametrically. The defined pickup dimensions are those of inductive pickups previously designed for PROSCAN at PSI. These are simple conducting wires of 1.8 mm diameter made of copper. We realize the large inductive loop by connecting the copper wire to the inner conductor through the outer conductor (of the coaxial section) and the small loop with the outer conductor (of the coaxial section) forming a rectangular loop shape as shown in Figure 2.10.

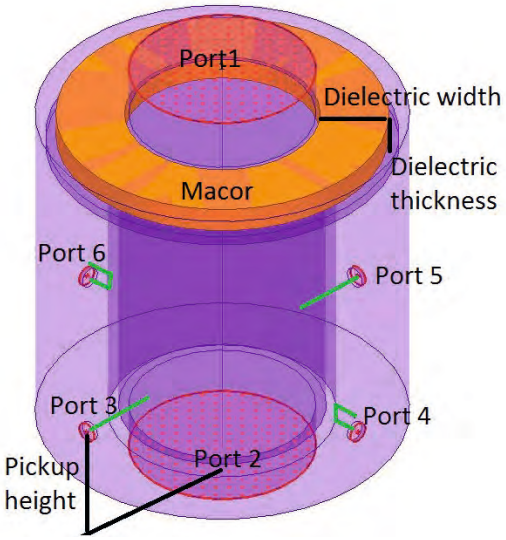

Figure 2.10: Geometry of the resonator. The surface of the model is assigned with aluminum conductivity. Waveport excitation is assigned on all ports with impedance termination of 366 Ω (coaxial impedance of the stretched wire with the beam pipe) for ports 1 and 2 (beam entrance and exit). All the measurement ports are normalized with 50 Ω impedance. Ports 3 and 5 represent the large inductive loops. Ports 4 and 6 the small loops. All the loops are at the same height.

Boundary conditions

By applying finite conducting boundary conditions to the model, an imperfect E boundary is defined. Based on the material properties for this boundary, HFSS calculates the loss as a function of frequency. HFSS forces the tangential E-field such that $E_{tan} = Z_s(\hat{n} \times H_{tan})$

- E_{tan} is the E field component tangential to the surface
- H_{tan} is the H field component tangential to the surface
- Z_s is the complex surface impedance of the boundary

Excitations

A thin wire with a cross-section of 0.2 mm with perfect electric conductor definition (for qualitative and quantitative calculations) represents the beam analogon. Because of the perfect electric conductor definition, the electric field is perpendicular to the thin wire surface. For each port, waveport excitations are assigned as HFSS assumes the model to be enclosed in a conductive shield. This means that waveport excitations need to be defined at the locations where energy enters and leaves the system, this includes the beam entrance, beam exit, and the pickup loops. With the assignment of the waveport excitation, HFSS considers each waveport as a semi-infinitely long coaxial port with the same cross-section. The impedance assigned on the beam entrance and the exit is the characteristic impedance of the coaxial line between the beam analogon and the beam pipe. The measurement ports are assigned a 50 Ω impedance. For every waveport excitation, we also have to define the number of modes and the type of modes allowed inside the model by defining an integration line.

Analysis setup

The analysis is performed for two different cases:

- with the beam analog: to optimize pickup position and ceramic dimensions
- without beam analog: to simulate mutual coupling between pickups and evaluate loaded Q-factor of the cavity

The analysis setup is summarized in Table 2.3. HFSS employs adaptive meshing by searching for the biggest error in the electric field gradients and sub-dividing the mesh in those regions. HFSS compares the S-parameters between consecutive passes and the model is considered converged when the maximum $\Delta S \leq 0.02$ dB is reached as mentioned in Table 2.3. The resonator is a narrow-band device, due to which, the adaptive solution frequency is set as a sinewave whose frequency is the design resonance frequency of 145.7 MHz. In order to evaluate the 3 dB

bandwidth of the final resonator model, a frequency sweep is defined over the range 130-161.4 MHz such that the center frequency is the resonance frequency.

Table 2.3: Driven Modal solution setup and Frequency sweep conditions.

Driven Modal Analysis setup	
Solution Frequency	145.7 MHz
Maximum No of passes (Adaptive)	20
Maximum ΔS (Adaptive)	0.02 dB
Initial mesh options	λ refinement
Maximum Refinement per pass (Adaptive)	20%
Order of Basis functions	2nd
Maximum ΔZ_o	2%
Frequency Sweep (Fast)	130-161.4 MHz (0.1 MHz step size)
Parametric investigation	Pickup position, Ceramic width, Ceramic thickness

The parametric investigation of the ceramic dimensions and pickup positions is performed with the beam analog in the model. S_{ji} plots (j - large pickup loops and i - beam entrance port) are used to determine design parameters of the optimized cavity resonator. The optimized model is shown in Figure 2.11 and in Table 2.4 is summarized for the design values of the cavity resonator tuned to 145.7 MHz.

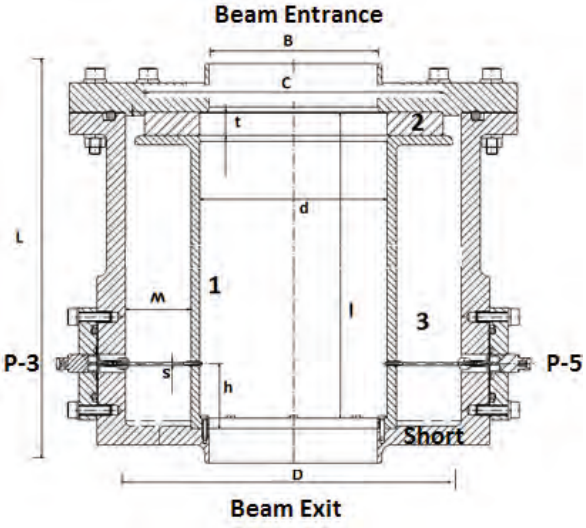

Figure 2.11: Dielectric-filled reentrant cavity resonator as a beam current monitor. P-3 and P-5 are the large inductive pickups. P-4 and P-6 are small pickups in the other plane.

Table 2.4: Parametric dimensions of the prototype.

Parameters	[mm]	Parameters	[mm]
B, Beam pipe diameter	90	M, inductive zone width	35
C, External diameter of the ring	160	t, dielectric thickness	12.425
d, Inner diameter of the inner cylinder	100	s, pickup diameter	1.8
L, Overall length	221	l, internal length	171
D, Inner diameter of the outer cylinder	180	h, pickup height	35

NOTE: All the following S_{ji} plots are between beam entrance and a large pickup. The unused pickup ports are terminated with a 50 Ω impedance and the beam entrance and exit ports with the characteristic impedance of the coaxial line between beam analog and beam pipe.

Ceramic width and thickness

Here, we investigate the influence of dielectric dimensions (ceramic width and thickness) on the resonance frequency and the signal coupling.

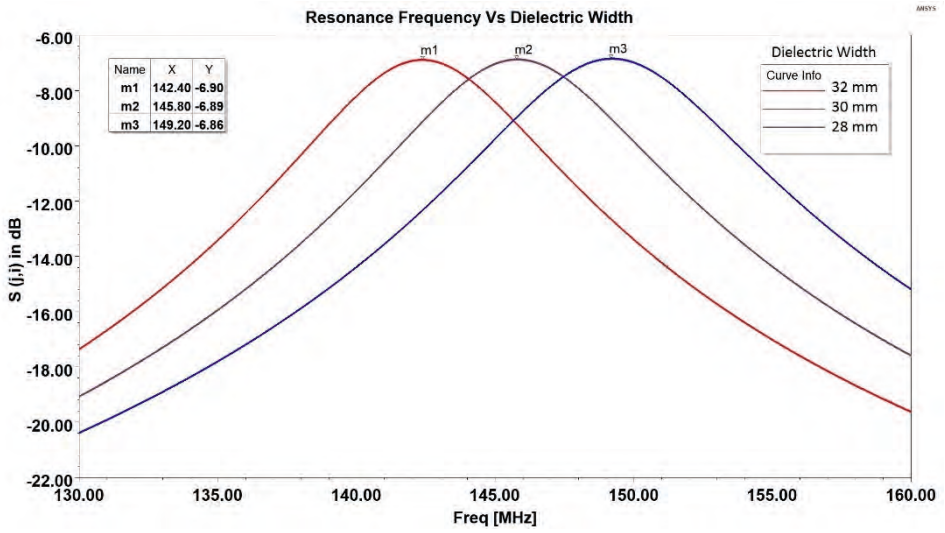

Figure 2.12: S_{ji} transmission plots of a large pickup loop with respect to the beam entrance port as a function of frequency for multiple dielectric widths (for a given dielectric thickness). Markers represent the resonance frequencies and the coupling coefficients at different dielectric widths. The resonance frequency is inversely proportional to the dielectric width.

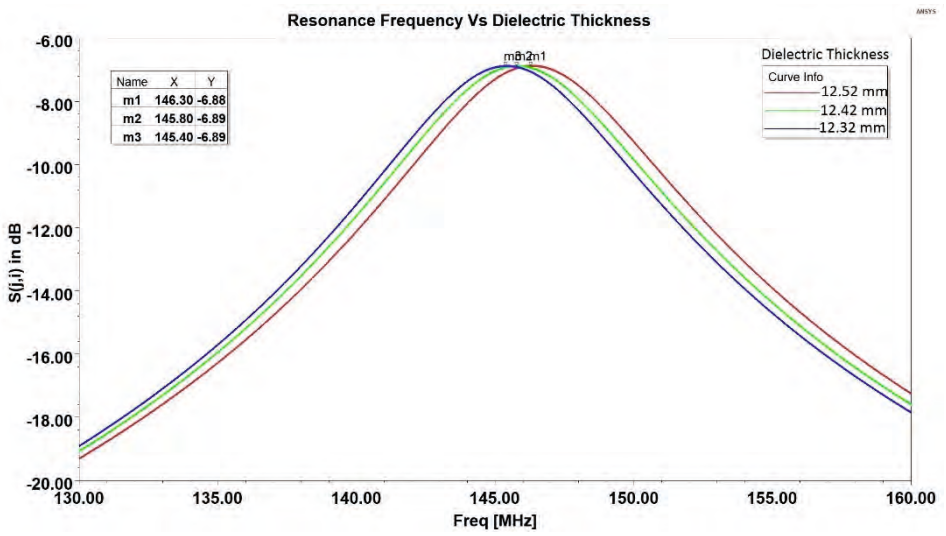

Figure 2.13: S_{ji} transmission plots of a large pickup loop with respect to the beam entrance port as a function of frequency for multiple dielectric thicknesses. Markers represent the resonance frequencies and the coupling coefficients. The resonance frequency is directly proportional to the dielectric thickness.

We evaluate the optimized dielectric dimensions of the macor ring from the effect of the dielectric width (Figure 2.12) and dielectric thickness (Figure 2.13) analysis on the system properties. For a given thickness, increasing the dielectric width increases the capacitance, which results in a decrease in the resonance frequency. On the contrary, for a given dielectric width, increasing the thickness decreases the capacitance, which increases the resonance frequency. Both of these behaviors are observable as expected. Moreover, we observe that the dimensions of the dielectric do not noticeably influence the beam- pickup coupling coefficient. This indicates that dielectric rings of different cross-sectional widths, for a given thickness, can be used to tune the resonance frequency without compromising the level of the extracted signal.

The dielectric dimensions: **width=30 mm** (ring outer radius=50+30 mm), **thickness=12.42 mm** are considered the optimal dimensions of the macor ring.

Pickup position

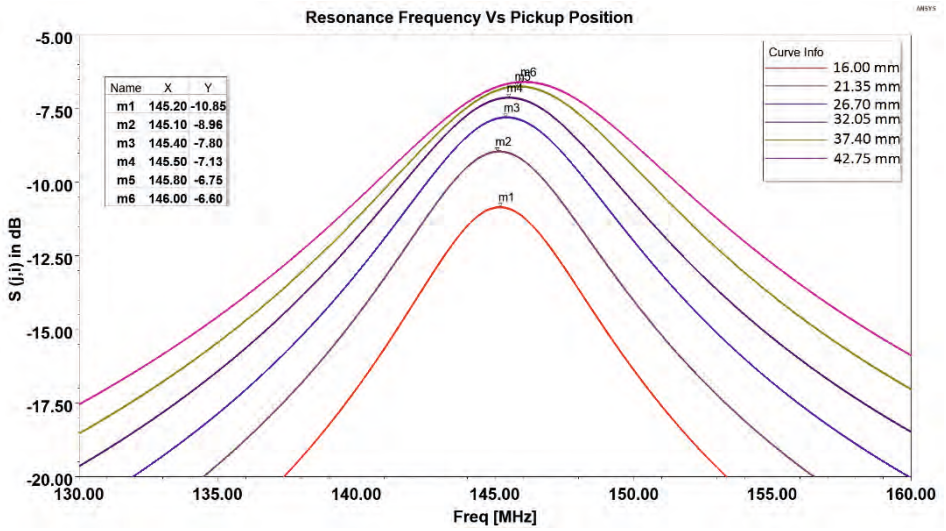

Figure 2.14: S_{ji} transmission plots of a large pickup loop with respect to the beam entrance port as a function of frequency for multiple pickup height (dimension 'h' in Figure 2.11). Markers represent the resonance frequencies and the coupling coefficients. Signal level increases with increasing pickup height as expected and results in a decreasing loaded quality factor consequently.

We study the influence of the pickup position on resonance frequency, Q factor, and S-parameters as plotted in Figure 2.14. From Figure 2.14, we observe two behaviors:

- Increasing the height of the pickup increases the resonance frequency minimally. An increase in the pickup height by a factor ~2.5 increases the resonance frequency by approximately 800 kHz.
- Increasing the pickup height increases the signal coupling, i.e., S_{31} and consequently, the loaded quality factor decreases. A lower loaded quality factor means a lower external quality factor and as per Eq (2.20), this should result in a higher signal level. This is because, as we increase the pickup height, we are lowering the Q_{ex} by coupling out more power as per Eq (2.10). For pickup height > 35 mm, the beam-pickup coupling does not increase significantly but the Q_L is lowered considerably.

The **pickup position = 35 mm** is chosen for all the pickup loops in the prototype. The S_{31} (port 3 (large pickup loop) for the beam at port 1), which provides the beam-pickup coupling for a centered beam analog in the final resonator model (i.e., with chosen dielectric dimensions and pickup position) is -6.83 dB at 145.7 MHz. The output voltage from the loop for a given beam equivalent current

through the beam analog can be evaluated from the above S_{31} coefficient. Since the characteristic impedance of the beam analog-beam pipe coaxial equivalent ($Z_{10} = 366\ \Omega$) and the port impedance ($Z_{port} = 50\ \Omega$) are not the same, the transfer impedance between the beam entrance port and the pickup port is given by

$$Z_{31} = |S_{31}| \sqrt{Z_{10} Z_{port}} \tag{2.25}$$

The S-matrix for the beam analog model is given in the Appendix.

For instance, for a sinewave with an amplitude of 1nA and a frequency of 145.7 MHz at port 1 as a source of excitation, we can expect the pickup voltage approximately as 61 nV. For a bunch with a repetition rate of 72.85 MHz and a rectangular bunch length of 2 ns, the amplitude of the second harmonic component (i.e., 145.7 MHz) constitutes approximately 25% of beam current. Thus, for an actual beam current of 4nA at 72.85 MHz, the pickup will return the signal level of 61 nV.

Mutual Pickup coupling

The intra-pickup coupling between a large pickup and a small pickup (for example, between port 3 and 4) of the final design of the resonator is shown in Figure 2.15. One of the ports is driven and the remaining unused pickup ports are terminated with 50 Ω port impedance for the simulation. The loaded quality factor Q_L is evaluated as per Eq (2.12). The loaded quality factor (Q_L), the resonance frequency, and peak coefficients (dB) for every pickup combination over 50 Ω port impedance is summarized in Table 2.5.

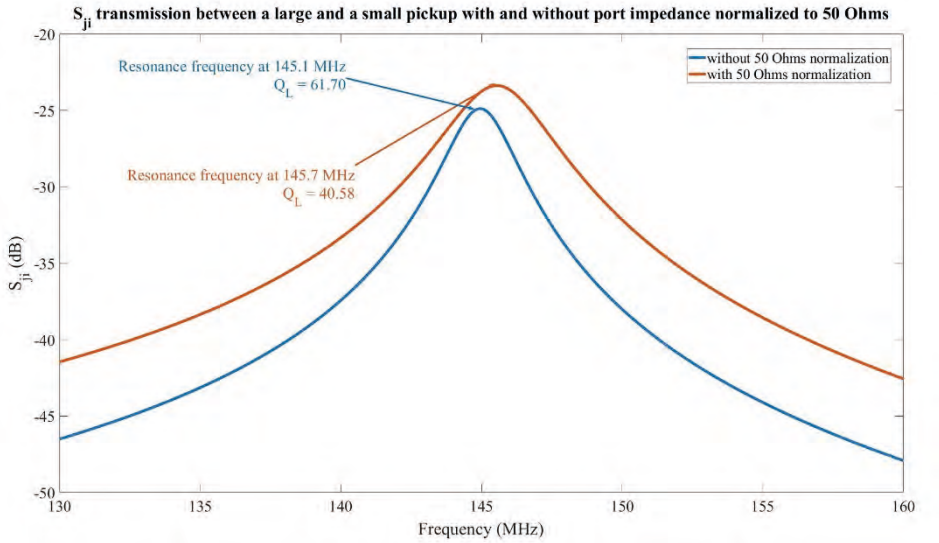

Figure 2.15: S_{ji} transmission plots for no-beam analog simulation (a measurement of mutual coupling between a large and a small loop) with and without port impedance normalized to 50 Ω (for all the ports of the cavity). With the 50 Ω impedance, the resonance frequency is 145.7 MHz with a loaded quality factor of 40.58. Without normalized port impedance (when the impedance is the characteristic impedance of the coaxial port of the pickup), the resonance frequency is 145.1 MHz with a loaded quality factor of 61.70.

The effect of 50 Ω normalization on the coupling coefficient is clearly seen in the above figure by comparing the mutual coupling (between a large and a small pickup) without the 50 Ω termination. It is important to remember, this does not take into effect the losses associated with cables, which will be used for the measurement. By terminating with 50 Ω, we observe the transmission between a large and a small pickup has increased which results in lowering of the Q_L and Q_{ex}.

Table 2.5: Simulated S-parameter coupling between pickup combinations for the resonator tuned to 145.7 MHz. Mentioned also the simulated loaded Q for all these combinations.

S-parameter	Resonance Frequency (MHz)	S-peak (dB)	Q-Value
S-34	145.7	-23.38	40.58
S-35	145.7	-1.53	40.58
S-36	145.7	-23.38	40.58
S-45	145.7	-23.38	40.58
S-46	145.7	-45.22	40.58
S-56	145.7	-23.38	40.58

Field plots

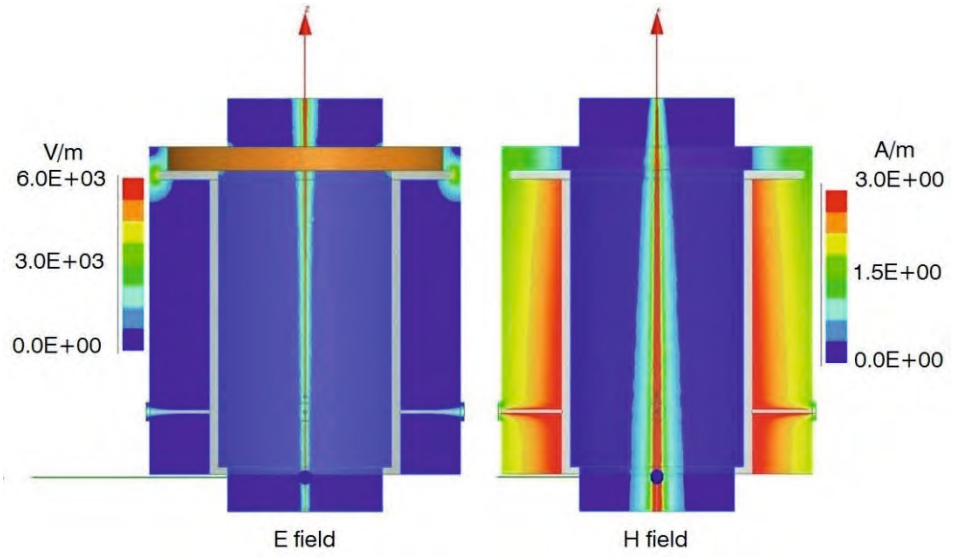

Figure 2.16: E and H fields induced inside the LC resonator (with the beam analog) at 145.7 MHz. The maximum E field is in the same plane as the maximum E of the beam. The same is the case for the H-field.

2.5 Analytical vs Simulation of the pickup amplitude

For the analytical evaluation of the pickup voltage from the inductive loops of the beam current monitor prototype, we use the loaded and unloaded Q factor of the prototype from the HFSS simulation results.

Values of parameters that we use for the evaluation is as follows:

ε_r, dielectric constant of macor = 6.0

Beam current = 1×10^{-9} A

Bunch repetition rate = 72.85×10^{6} Hz; period = 13.72×10^{-9} s

Bunch duration = 2×10^{-9} s

For a given beam intensity, we can evaluate the total number of charged particles in the 2 ns bunch at 1 nA beam intensity using the formula:

$$I_{beam} = eN / dt$$
$$N = I_{beam} dt / e \approx 86 protons \quad (2.26)$$

Hence, the bunch charge q

$$q = Ne = 1.36\times10^{-17} C \quad (2.27)$$

Taking the dimensions of the macor ceramic from Table 2.4

r_{max} is the outer radius of the dielectric ring = 80 mm

r_{min} is the inner radius of the dielectric ring = 50 mm

d is the dielectric thickness = 12.425 mm

Then, C_{gap} yields 50 pF (approximately) as per Eq (2.4).

To determine the pickup voltage for a given beam intensity, we need to calculate R1, the shunt impedance of the resonator at the resonance frequency ω_o. This we evaluate as:

$$Q_o = \omega_o R1 C_{gap} \tag{2.28}$$

According to the HFSS Eigenmode solver simulation, Q_o = 267. Substituting Q_o in the above formula, we evaluate the shunt impedance as R1 = 5865 Ω. The quantity defined as $R1/Q_o$ is a figure of merit for the shape of the cavity is independent of the choice of material, which yields 22 Ω.

We take Q_L of the cavity resonator as 40.6 from the HFSS Driven modal S-parameter solutions (mutual pickup coupling). We then evaluate Q_{ext} as 47.3 as per Eq (2.10). Now, substituting all the terms in the Eq (2.20) provides pickup voltage for 1nA beam intensity with a repetition rate of 72.85 MHz as per

$$V_{out} \equiv \omega_o q \sqrt{\frac{Z}{Q_{ex}} \frac{R1}{Q_o}} \exp(-\omega_o^2 \sigma_z^2 / 2\beta^2 c^2) \approx 11 \text{ nV}$$

This shows the agreement between the simulation estimate of 15 nV and the analytical estimate is satisfactory.

2.6 Conclusion

A dielectric-filled reentrant coaxial cavity has been designed such that its fundamental mode of resonance is at 145.7 MHz. The induced E and B fields in the separate transmission lines of the cavity represent a TEM mode configuration, but what we have really is a quasi-TEM. Since the field solutions of the TEM_1 mode in the capacitive region (dominant) and of the TM_{010} mode in a pillbox are the same and as confirmed by the reasonable agreement between the simulation and TM_{010} mode analytical estimate, this cavity will be further on referred to as TM_{010} (monopole) mode cavity.

2.7 Cut-plane of the prototype resonator

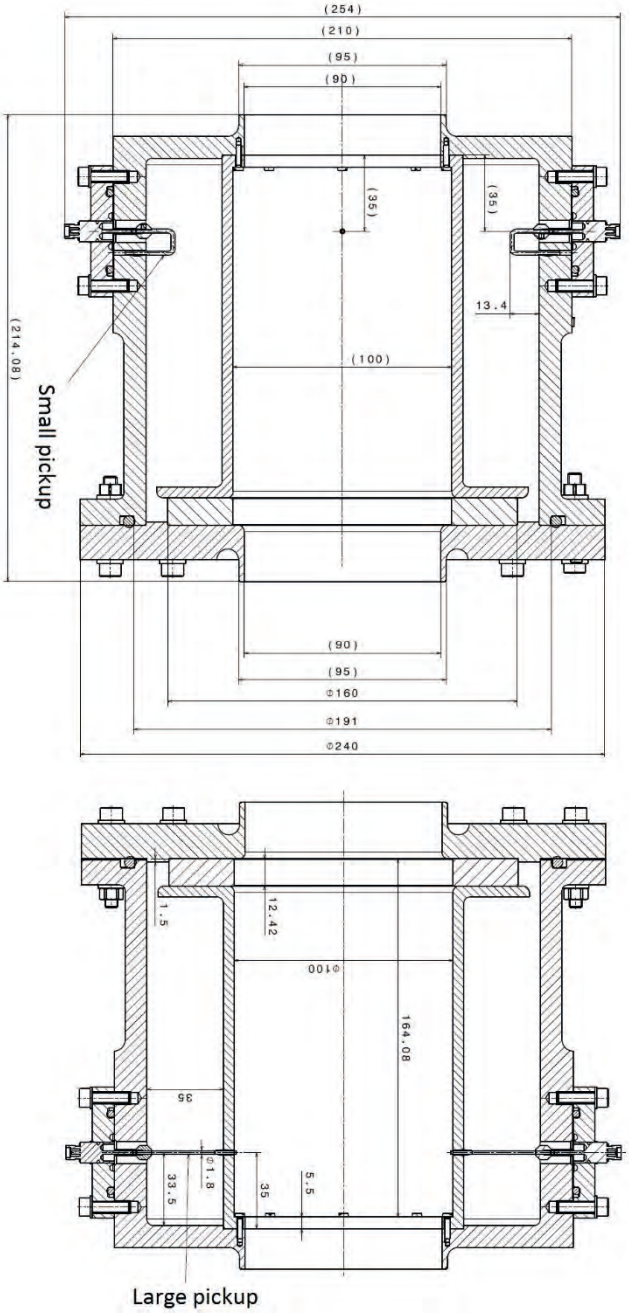

2.8 Appendix

Frequency		S:1:1	S:1:2	S:1:3	S:1:4	S:1:5	S:1:6
145.7 MHz	S:1:1	0.457	0.545	0.455	0.037	0.456	0.037
	S:1:2	0.545	0.453	0.457	0.037	0.457	0.037
	S:1:3	0.455	0.457	0.543	0.037	0.457	0.037
	S:1:4	0.037	0.037	0.037	0.996	0.037	0.003
	S:1:5	0.456	0.457	0.457	0.037	0.542	0.037
	S:1:6	0.037	0.037	0.037	0.003	0.037	0.996

2.9 References

[1] Gerigk F. Cavity types. CAS - Cern Accel. Sch. RF Accel., Ebeltoft: 2010, p. 277–98. https://doi.org/10.5170/CERN-2011-007.277.

[2] Humphries S. Principles of Charged Particle Acceleration, 1999, p. 356–407.

[3] Griffiths DJ. Introduction To Electrodynamics. Third Edit. New Jersey: Prentice Hall; 1999.

[4] Jensen E. RF Cavity Design. CAS - Cern Accel. Sch., 2007, p. 1–73. https://doi.org/10.5170/CERN-2014-009.405.

[5] Lipka D. Cavity Bpm Designs , Related Electronics and Measured Performances. Proc. DIPAC09, 2009, p. 280–4.

[6] Srinivasan S, Duperrex P-A. Dielectric-Filled Reentrant Cavity Resonator as a Low-Intensity Proton Beam Diagnostic. Instruments 2018;2:24. https://doi.org/10.3390/instruments2040024.

[7] Feynman R, Leighton R, Sands M. Cavity Resonators and Waveguides. Feynman Lect. Phys. Vol.2 Mainly Electromagn. Matter, vol. II, New York: Basic Books; 2011, p. 23.1-24.12.

[8] Simon C, Luong M, Chel S, Napoly O, Novo J, Roudier D, et al. Performance of a reentrant cavity beam position monitor. Phys Rev Spec Top - Accel Beams 2008;11:1–10. https://doi.org/10.1103/PhysRevSTAB.11.082802.

[9] Russer P. Transmission Lines and Waveguides. Electromagn. Microw. Circuit, Antenna Des. Commun. Eng. Second Edi, Artech House; n.d.

[10] Zhang K, Li D. Metallic Waveguides and Resonant Cavities. Electromagn. Theory Microwaves Optoelectron., 2007, p. 235–316. https://doi.org/10.1007/978-3-540-74296-8_5.

[11] Microwave Phase Modulators for Smoothing by Spectral Dispersion. LLE Rev n.d.;68:192–208.

[12] Young PH. Electronic Communication Techniques. Second Int. Merill, Columbus; 1991.

[13] Luo Q, Sun BG, Zhou ZR, Jia QK. Design And Cold Test Of Re-entrant Cavity Bpm For HlS *. Proc. 2011 Part. Accel. Conf. New York, USA, 2011, p. 420–2.

[14] Puglisi M. Conventional RF cavity design. CAS - Cern Accel Sch 1992.

[15] Collin RE. Foundations for Microwave Engineering. Wiley-Interscience,

New York; 2001.

[16] C.G. Montgomery; E. M. Purcell; R. H. Dicke. Principles of Microwave Circuits. New York Dover; 1965.

[17] Kajfez D. Q factor. Oxford MS, Vector Fields; 1994.

[18] Kajfez D, Chebolu S, Kishk AA. Uncertainty analysis of the transmission-type measurement of Q-factor. IEEE Trans Microw Theory Tech 1999;47:367–71. https://doi.org/10.1109/22.750244.

[19] Wilson PB. Introduction to wakefields and wake potentials. AIP Conf. Proc. 184, 1989, p. 525–64. https://doi.org/10.1063/1.38045.

[20] Frédéric de Coulon. Théorie Et Traitement Des Signaux. Laussane: 1984.

[21] ANSYS HFSS 2017. http://www.ansys.com/products/electronics/ansys-hfss/hfss-capabilities#cap2.

[22] Weibler J. EMC TEST and DESIGN. 1993.

[23] Macor Machinable Glass Ceramic Properties 2017. http://accuratus.com/Macormats.html.

[24] © 2005 Ansoft Corporation. High Frequency Structure Simulator. REV1-0 ed. 2005.